Journal of Systems Engineering and Electronics
Vol. 35, No. 1, February 2024, pp.31 – 42

Persymmetric adaptive polarimetric detection of subspace range-spread targets in compound Gaussian sea clutter

XU Shuwen[1,*], HAO Yifan[2], WANG Zhuo[3], and XUE Jian[4]

1. National Key Laboratory of Radar Signal Processing, Xidian University, Xi'an 710071, China; 2. Xi'an Electronic Engineering Research Institute, Xi'an 710100, China; 3. Beijing Institute of Radio Measurement, Beijing 100039, China; 4. School of Communications and Information Engineering, Xi'an University of Posts and Telecommunications, Xi'an 710121, China

Abstract: This paper focuses on the adaptive detection of range and Doppler dual-spread targets in non-homogeneous and non-Gaussian sea clutter. The sea clutter from two polarimetric channels is modeled as a compound-Gaussian model with different parameters, and the target is modeled as a subspace range-spread target model. The persymmetric structure is used to model the clutter covariance matrix, in order to reduce the reliance on secondary data of the designed detectors. Three adaptive polarimetric persymmetric detectors are designed based on the generalized likelihood ratio test (GLRT), Rao test, and Wald test. All the proposed detectors have constant false-alarm rate property with respect to the clutter texture, the speckle covariance matrix. Experimental results on simulated and measured data show that three adaptive detectors outperform the competitors in different clutter environments, and the proposed GLRT detector has the best detection performance under different parameters.

Keywords: sea clutter, adaptive polarimetric detection, compound Gaussian model, subspace range-spread target, persymmetric structure.

DOI: 10.23919/JSEE.2023.000133

1. Introduction

Adaptive detection of radar targets based on characteristics of sea clutter has been a research hotspot in the radar field. The complexity of clutter and the concealment of new-type targets are major factors affecting the performance of the target detection. In order to improve the ability of radar target detection in sea clutter, it is important to understand the statistical property of sea clutter and to design an effective detection method.

In the early years, the Gaussian model was proposed to describe the low-resolution radar sea clutter, according to the central limit theorem [1,2]. For the high-resolution radar, the number of scatters is reduced in a radar range resolution cell. In this case, although the local backscattering from each sea surface resolution cell still satisfies the central limit theorem (CLT), the sea clutter presents non-Gaussianity, which results from the spatial and temporal texture modulations of the large-scale structure (refer to as gravity waves) on the local Gaussian speckle (refer to as capillary waves) [3]. Based on the scattering mechanism of the sea surface, a two-component compound-Gaussian (CG) model was proposed to describe non-Gaussian sea clutter [4]. The commonly used CG distributions of sea clutter contain the K distribution [5−7], the generalized Pareto (GP) distribution [8], the CG distribution with inverse Gaussian (CG-IG) [9], and the CG distribution with generalized IG (CG-GIG) [10].

Based on the sea clutter models, some ad-hoc detectors have been proposed to detect radar targets [11]. These detection algorithms are designed to exploit the radar echo data from only one single polarimetric channel. Therefore, they usually have poor performances to detect weak targets due to the lack of multi-channel polarimetric information. In order to solve this problem, the polarimetric diversity technology has been widely used to improve radar performance in recent years. Different polarimetric characteristics between sea clutter and target signals provide a way to improve the detection performance of radar targets. Kelly's generalized likelihood ratio test (GLRT) was extended to the multi-polarimetric domain, and the polarimetric space-time generalized likelihood ratio (PST-GLR) detector was derived by using one-step GLRT in Gaussian clutter [12]. A polarimetric adaptive matched filter [13] was proposed to process the information of two polarimetric channels based on two-step GLRT, which requires less computation than PST-

Manuscript received October 14, 2022.
*Corresponding author.
This work was supported by the National Natural Science Foundation of China (62371382;62071346), the Science, Technology & Innovation Project of Xiong 'an New Area (2022XAGG0181), and the Special Funds for Creative Research (2022C61540).

GLR detector. The detectors designed based on the Gaussian clutter model will suffer severe performance degradation in the heavy-tailed non-Gaussian sea clutter. Therefore, a CG model [14] was introduced into the design of the polarimetric adaptive detector and proposed a texture-free GLRT (TF-GLRT), which uses radar echoes of two polarimetric channels. The Wald and Rao tests were proposed to design polarimetric detectors for radar target detection [15].

The above detectors are designed for point-like targets, which always only occupy a single range cell. When a target is illuminated by high-resolution radar, it is usually divided into multiple scattering centers, its echoes are distributed on multiple continuous range cells [16−18]. This kind of target is named as a "range-spread target". In addition, the high-resolution radar can also observe the motion postures of different parts of a target, so the target echoes may have the Doppler spread behavior. Therefore, it is more practical to model the target echo as a multi-rank linear subspace range spread target. Many researchers proposed some algorithms to detect the multi-rank linear subspace range spread target. For example, Guan et al. [16] proposed a subspace range-spread target adaptive detection algorithm that utilized the GLRT in CG clutter and radar echoes from a single polarimetric channel. Alfano et al. [19] proposed a GLRT detector, a Wald detector, and a detector without secondary data for the rank-one range spread target by using multi-polarimetric channels and the CG clutter model.

The performance of adaptive detectors can be affected by the number of secondary cells. The Reed, Mallett, and Brennan (RMB) criterion [20] shows that, when the number of secondary cells is more than twice the number of accumulated pulses, the adaptive loss of the detection algorithm compared with the theoretical optimal performance can reach an acceptable range.

In practice, it is impossible to obtain enough secondary cells when the sea clutter distribution is heterogeneous. To solve this problem, a polarimetric covariance matrix model was established by using polarimetric prior information in [21], which reduces the dependence on the secondary data. In addition, a detector using the persymmetric property of the clutter covariance matrix was proposed in [22], which effectively improves the detection performance when the secondary data are insufficient.

The utilization of the polarimetric information can improve the detection performance of radar targets in sea clutter [23]. And, the use of the persymmetric property of the covariance matrix can reduce the dependence on the secondary data [24]. Therefore, in this paper, we address the problem of adaptive polarimetric detection for radar targets in non-Gaussian and non-homogeneous sea clutter with an unknown covariance matrix. The main contributions of this paper are summarized as follows.

(i) A complex model is used to model the radar target and sea clutter in order to make the designed detector more practical. The target is modeled as a multi-rank subspace model, and the clutter speckle covariance matrix is modeled as a persymmetric matrix.

(ii) Three adaptive polarimetric detectors are proposed based on the two-step GLRT test, Rao test, and Wald test. Simulation results show that the three detectors have less dependence on the secondary data and have the best detection performance in different parameters.

(iii) The proposed three detectors have constant false alarm rate (CFAR) property with respect to clutter the texture distribution, and the approximate CFAR property with the respect to speckle covariance matrix.

The remainder of this paper is organized as follows. The target and sea clutter models are presented in Section 2. Three polarimetric detectors are developed on the basis of the two-step versions of the GLRT, Wald, and Rao tests in Section 3. The performance analysis of the proposed detectors is provided in Section 4. Finally, the conclusions are drawn in Section 5.

2. Detection problem description

Assuming that radar echoes are collected from N consecutive coherent pulses by two polarimetric channels (HH and HV) in a coherent processing interval (CPI). The range spread target to be detected occupies H range cells, which are called the cells under test (CUTs), and the data in CUTs are named as primary data. There are K reference cells around CUTs and the data in the reference cells are called as secondary data. The returns from two polarimetric channels on the kth range cell can be denoted by $N\times 1$ dimensional complex vectors $\boldsymbol{x}_{\mathrm{HH},k}$ and $\boldsymbol{x}_{\mathrm{HV},k}$. The echo signals of two polarimetric channels are arranged as $\boldsymbol{x}_k=(\boldsymbol{x}_{\mathrm{HH},k}^{\mathrm{T}},\boldsymbol{x}_{\mathrm{HV},k}^{\mathrm{T}})^{\mathrm{T}}$. The range spread target detection problem in sea clutter can be formulated in terms of the following binary hypothesis test:

$$\mathrm{H}_0:\begin{cases}\boldsymbol{x}_i=\boldsymbol{c}_i,\ i=1,2,\cdots,H\\ \boldsymbol{x}_k=\boldsymbol{c}_k,\ k=H+1,H+2,\cdots,H+L\end{cases}\tag{1}$$

$$\mathrm{H}_1:\begin{cases}\boldsymbol{x}_i=\boldsymbol{s}_i+\boldsymbol{c}_i,\ i=1,2,\cdots,H\\ \boldsymbol{x}_k=\boldsymbol{c}_k,\ k=H+1,H+2,\cdots,H+L\end{cases}\tag{2}$$

where H_0 denotes the hypothesis that the target is absent, and H_1 represents that the target is present. The reference cells only contain sea clutter collected from the both sides of CUTs, which are independent identically distributed (IID) and have the same speckle covariance matrix as sea clutter in CUTs.

In a radar CPI, the sea clutter sequence can be modeled as a spherical invariant random vector. The clutter vectors $\boldsymbol{c}_{\mathrm{HH},i}$ and $\boldsymbol{c}_{\mathrm{HV},i}$ from the two polarimetric channels are given by

$$\begin{cases}\boldsymbol{c}_{\mathrm{HH},i}=\sqrt{\tau_{\mathrm{HH},i}}\boldsymbol{u}_{\mathrm{HH},i}\\ \boldsymbol{c}_{\mathrm{HV},i}=\sqrt{\tau_{\mathrm{HV},i}}\boldsymbol{u}_{\mathrm{HV},i}\end{cases},\ i=1,2,\cdots,H \tag{2}$$

where $\boldsymbol{u}_{\mathrm{HH},i}$ and $\boldsymbol{u}_{\mathrm{HV},i}$ denote speckle components and are modeled as N-dimensional complex Gaussian random vectors with zero mean, $\tau_{\mathrm{HH},i}$ and $\tau_{\mathrm{HV},i}$ denote texture components and are non-negative random constants. The clutter covariance matrix in the HH polarimetric channel is

$$\boldsymbol{M}_{\mathrm{HH}}=\mathrm{E}[\boldsymbol{c}_{\mathrm{HH}}\boldsymbol{c}_{\mathrm{HH}}^{\mathrm{H}}]=\tau_{\mathrm{HH}}\mathrm{E}[\boldsymbol{u}_{\mathrm{HH}}\boldsymbol{u}_{\mathrm{HH}}^{\mathrm{H}}]=\tau_{\mathrm{HH}}\boldsymbol{R}_{\mathrm{HH}} \tag{3}$$

where $\boldsymbol{R}_{\mathrm{HH}}$ is the speckle covariance matrix, and $(\cdot)^{\mathrm{H}}$ represents the matrix conjugate transposition operation. The covariance matrix of the radar echoes in the two polarimetric channels can be given by $\boldsymbol{M}_i=\mathrm{E}[\boldsymbol{c}_i\boldsymbol{c}_i^{\mathrm{H}}]=\boldsymbol{\Gamma}_i\boldsymbol{R}\boldsymbol{\Gamma}_i$, where $\boldsymbol{R}$ denotes the speckle's covariance matrix,

$$\boldsymbol{\Gamma}_i=\begin{bmatrix}\tau_{\mathrm{HH},i}&0\\0&\tau_{\mathrm{HV},i}\end{bmatrix}\otimes\boldsymbol{I}_N. \tag{4}$$

The sea clutter in HH and HV channels is assumed to be independent [25], and thus

$$\boldsymbol{R}=\begin{bmatrix}\boldsymbol{R}_{\mathrm{HH}}&\boldsymbol{0}\\\boldsymbol{0}&\boldsymbol{R}_{\mathrm{HV}}\end{bmatrix}. \tag{5}$$

The signal $\boldsymbol{s}_i=(\boldsymbol{s}_{i,\mathrm{HH}}^{\mathrm{T}},\boldsymbol{s}_{i,\mathrm{HV}}^{\mathrm{T}})^{\mathrm{T}}$ of range and Doppler dual-spread target [16] can be expressed as

$$\boldsymbol{s}_{i,\mathrm{Pol}}=\boldsymbol{E}_i\boldsymbol{a}_{i,\mathrm{Pol}},\ i=1,2,\cdots,H;\mathrm{Pol}=\mathrm{HH,HV} \tag{6}$$

where $\boldsymbol{s}_{i,\mathrm{Pol}}=[s_{i,\mathrm{Pol}}(1),s_{i,\mathrm{Pol}}(2),\cdots,s_{i,\mathrm{Pol}}(N)]$ denotes the target echoes from HH or HV polarimetric channel, and $\boldsymbol{a}_{i,\mathrm{Pol}}=[a_{i,\mathrm{Pol}}(1),a_{i,\mathrm{Pol}}(2),\cdots,a_{i,\mathrm{Pol}}(N_i)]$ represents the complex amplitude of the N_i scatters in the HH or HV polarimetric channel at the ith CUT, the steering matrix $\boldsymbol{E}_i$ is

$$\boldsymbol{E}_i=\begin{bmatrix}\exp\{\mathrm{j}2\pi f_{i,1}\}&\exp\{\mathrm{j}2\pi f_{i,2}\}&\cdots&\exp\{\mathrm{j}2\pi f_{i,N_i}\}\\ \exp\{\mathrm{j}2\pi\times 2f_{i,1}\}&\exp\{\mathrm{j}2\pi\times 2f_{i,2}\}&\cdots&\exp\{\mathrm{j}2\pi\times 2f_{i,N_i}\}\\ \vdots&\vdots&&\vdots\\ \exp\{\mathrm{j}2\pi\times Nf_{i,1}\}&\exp\{\mathrm{j}2\pi\times Nf_{i,2}\}&\cdots&\exp\{\mathrm{j}2\pi\times Nf_{i,N_i}\}\end{bmatrix}_{N\times N_i} \tag{7}$$

where $f_{i,k}$ represents the normalized Doppler frequency of the kth scatterer at the ith range cell.

Equation (6) can be rewritten by taking the singular value decomposition (SVD) of the steering matrix, $\boldsymbol{E}_i=\boldsymbol{U}_i\boldsymbol{\Lambda}_i\boldsymbol{V}_i$. Thus, the target signal can be rewritten by

$$\boldsymbol{s}_{i,\mathrm{Pol}}=\boldsymbol{U}_i\boldsymbol{b}_{i,\mathrm{Pol}},\ i=1,2,\cdots,H;\mathrm{Pol}=\mathrm{HH,HV} \tag{8}$$

where $\boldsymbol{b}_{i,\mathrm{Pol}}=\boldsymbol{\Lambda}_i\boldsymbol{V}_i\boldsymbol{a}_{i,\mathrm{Pol}}$, $\boldsymbol{U}_i$ is the $N\times N_i$ dimensional unitary matrix representing the left singular vector of $\boldsymbol{E}_i$, called the mode matrix; the elements in $\boldsymbol{b}_{i,\mathrm{Pol}}=[b_{i,\mathrm{Pol}}(1),(b_{i,\mathrm{Pol}}(2),\cdots,b_{i,\mathrm{Pol}}(N_i)]^{\mathrm{T}}$ denotes the mode weights. The target backscattered signal is located in the linear subspace $<\boldsymbol{U}_i>$ which is formed by the column vector of $\boldsymbol{U}_i$, and its position is determined by $\boldsymbol{b}_{i,\mathrm{Pol}}$; the number of scatters in the ith element determines the dimension of the linear subspace $<\boldsymbol{U}_i>$.

For the linear array receiving signals or the pulse sequence with the symmetric interval distribution, the clutter covariance matrix is persymmetric [22]. Thus, the covariance matrix $\boldsymbol{R}$ is a matrix with double symmetry and can be transformed to a real symmetric matrix $\tilde{\boldsymbol{R}}=\boldsymbol{W}^{\mathrm{H}}\boldsymbol{R}\boldsymbol{W}$ by a transformation matrix:

$$\boldsymbol{W}=\begin{cases}\dfrac{1}{\sqrt{2}}\begin{bmatrix}\boldsymbol{I}_{N/2}&\boldsymbol{Q}_{N/2}\\ \mathrm{j}\boldsymbol{I}_{N/2}&-\mathrm{j}\boldsymbol{Q}_{N/2}\end{bmatrix}, & \text{even}\\ \dfrac{1}{\sqrt{2}}\begin{bmatrix}\boldsymbol{I}_{(N-1)/2}&\boldsymbol{0}&\boldsymbol{Q}_{(N-1)/2}\\ \boldsymbol{0}&\sqrt{2}&\boldsymbol{0}\\ \mathrm{j}\boldsymbol{I}_{(N-1)/2}&\boldsymbol{0}&-\mathrm{j}\boldsymbol{Q}_{(N-1)/2}\end{bmatrix}, & \text{odd}\end{cases} \tag{9}$$

In this case, the radar echoes can be converted by the matrix $\boldsymbol{W}$, and the binary hypothesis test problem in (1) and (2) can be rewritten as

$$\mathrm{H}_0:\begin{cases}\tilde{\boldsymbol{x}}_i=\tilde{\boldsymbol{c}}_i=\boldsymbol{W}_{\mathrm{Pol}}\boldsymbol{c}_i\\ \tilde{\boldsymbol{x}}_k=\tilde{\boldsymbol{c}}_k=\boldsymbol{W}_{\mathrm{Pol}}\boldsymbol{c}_k\end{cases}, \tag{10}$$

$$\mathrm{H}_1:\begin{cases}\tilde{\boldsymbol{x}}_i=\tilde{\boldsymbol{s}}_i+\tilde{\boldsymbol{c}}_i=\boldsymbol{W}_{\mathrm{Pol}}\boldsymbol{s}_i+\boldsymbol{W}_{\mathrm{Pol}}\boldsymbol{c}_i\\ \tilde{\boldsymbol{x}}_k=\tilde{\boldsymbol{c}}_k=\boldsymbol{W}_{\mathrm{Pol}}\boldsymbol{c}_k\end{cases}, \tag{11}$$

where $\boldsymbol{W}_{\mathrm{Pol}}=I_2\otimes\boldsymbol{W}$, $i=1,2,\cdots,H$, $k=H+1,H+2,\cdots,H+L$.

The joint probability density function (PDF) of $\tilde{\boldsymbol{x}}_1,\tilde{\boldsymbol{x}}_2,\cdots,\tilde{\boldsymbol{x}}_H$ can be given by

$$f(\tilde{\boldsymbol{x}}_1,\tilde{\boldsymbol{x}}_2,\cdots,\tilde{\boldsymbol{x}}_H|\tau_{\mathrm{HH}},\tau_{\mathrm{HV}};\mathrm{H}_\gamma)=\prod_{i=1}^{H}\frac{1}{\pi^{2N}(\tau_{\mathrm{HH},i},\tau_{\mathrm{HV},i})^N\left|\tilde{\boldsymbol{R}}\right|}\cdot \exp(-\boldsymbol{\sigma}_i^{\mathrm{H}}(\tilde{\boldsymbol{X}}_i-\gamma\tilde{\boldsymbol{P}}_i\boldsymbol{B}_i)^{\mathrm{H}}\cdot\tilde{\boldsymbol{R}}^{-1}(\tilde{\boldsymbol{X}}_i-\gamma\tilde{\boldsymbol{P}}_i\boldsymbol{B}_i)\boldsymbol{\sigma}_i) \tag{13}$$

where $\gamma=0,1$ corresponds to H_0 and H_1, respectively. Then, $\boldsymbol{\sigma}_i=\mathrm{diag}\{1/\sqrt{\tau_{\mathrm{HH},i}},1/\sqrt{\tau_{\mathrm{HV},i}}\}^{\mathrm{T}}$, $\boldsymbol{\tau}_{\mathrm{HH}}=(\tau_{\mathrm{HH},1},\tau_{\mathrm{HH},2},\cdots,\tau_{\mathrm{HH},H})$, $\boldsymbol{\tau}_{\mathrm{HV}}=(\tau_{\mathrm{HV},1},\tau_{\mathrm{HV},2},\cdots,\tau_{\mathrm{HV},H})$, $\tilde{\boldsymbol{P}}_i=\boldsymbol{W}_{\mathrm{Pol}}\boldsymbol{I}_2\otimes\boldsymbol{U}_i$ and $\tilde{\boldsymbol{X}}_i=\begin{bmatrix}\boldsymbol{W}\boldsymbol{x}_{i,\mathrm{HH}}&\boldsymbol{0}\\ \boldsymbol{0}&\boldsymbol{W}\boldsymbol{x}_{i,\mathrm{HV}}\end{bmatrix}$, the speckle covariance matrix $\tilde{\boldsymbol{R}}=\boldsymbol{W}_{\mathrm{Pol}}^{\mathrm{H}}\boldsymbol{R}\boldsymbol{W}_{\mathrm{Pol}}$ is a real symmetric matrix, the target mode weight matrix is denoted by

$$\boldsymbol{B}_i=\left[\begin{array}{cc}\boldsymbol{b}_{i,\mathrm{HH}} & \boldsymbol{0}\\ \boldsymbol{0} & \boldsymbol{b}_{i,\mathrm{HV}}\end{array}\right]. \tag{14}$$

3. Design of polarimetric detectors for subspace range-spread targets

In this section, the two-step GLRT, Wald, and Rao tests are employed to design adaptive polarimetric detectors, respectively. First, we assume that the linear subspace $<\boldsymbol{U}_i>$ and its dimension N_i are known. In practical applications, based on the minimum description length criterion [26] or other model order selection methods [27,28], N_i can be determined， and then $<\boldsymbol{U}_i>$ can be estimated by super-resolution spectrum estimation methods such as multiple signal classification (MUSIC) and estimation of signal parameters using rotation invariance techniques (ESPRIT) [29].

3.1 Polarimetric detector based on the two-step GLRT

Assuming that $\tilde{\boldsymbol{R}}$ is known, the GLRT of the binary hypothesis test problem in (10) can be denoted as

$$\frac{\max\limits_{\boldsymbol{B}_1,\cdots,\boldsymbol{B}_i,\tau_{\mathrm{HH}},\tau_{\mathrm{HV}}} f(\tilde{\boldsymbol{x}}_1,\tilde{\boldsymbol{x}}_2,\cdots,\tilde{\boldsymbol{x}}_H|\tau_{\mathrm{HH}},\tau_{\mathrm{HV}};\mathrm{H}_1)}{\max\limits_{\tau_{\mathrm{HH}},\tau_{\mathrm{HV}}} f(\tilde{\boldsymbol{x}}_1,\tilde{\boldsymbol{x}}_2,\cdots,\tilde{\boldsymbol{x}}_H|\tau_{\mathrm{HH}},\tau_{\mathrm{HV}};\mathrm{H}_0)}\underset{\mathrm{H}_0}{\overset{\mathrm{H}_1}{\gtrless}}\eta. \tag{15}$$

The maximum likelihood estimate of $\boldsymbol{B}_i$ can be given by [14] as follows:

$$\boldsymbol{B}_i=\left(\tilde{\boldsymbol{P}}_i^{\mathrm{H}}\tilde{\boldsymbol{R}}^{-1}\tilde{\boldsymbol{P}}_i\right)^{-1}\tilde{\boldsymbol{P}}_i^{\mathrm{H}}\tilde{\boldsymbol{R}}^{-1}\tilde{\boldsymbol{X}}_i. \tag{16}$$

The maximum likelihood estimation of texture under two hypotheses [19] is defined as follows:

$$\begin{cases}\tau_{\mathrm{HH},i}^{(\gamma)}=\dfrac{1}{N}\boldsymbol{\Psi}_i^{(\gamma)}(1,1)\left(1+\dfrac{\mathrm{Re}\left\{\boldsymbol{\Psi}_i^{(\gamma)}(1,2)\right\}}{\sqrt{\boldsymbol{\Psi}_{i,11}^{(\gamma)}\boldsymbol{\Psi}_{i,22}^{(\gamma)}}}\right)\\ \tau_{\mathrm{HV},i}^{(\gamma)}=\dfrac{1}{N}\boldsymbol{\Psi}_i^{(\gamma)}(2,2)\left(1+\dfrac{\mathrm{Re}\left\{\boldsymbol{\Psi}_i^{(\gamma)}(1,2)\right\}}{\sqrt{\boldsymbol{\Psi}_i^{(\gamma)}(1,1)\boldsymbol{\Psi}_i^{(\gamma)}(2,2)}}\right)\end{cases} \tag{17}$$

where $\boldsymbol{\Psi}_i^{(\gamma)}=\tilde{\boldsymbol{X}}_i^{\mathrm{H}}[\tilde{\boldsymbol{R}}^{-1}-\gamma\tilde{\boldsymbol{R}}^{-1}\tilde{\boldsymbol{P}}_i(\tilde{\boldsymbol{P}}_i^{\mathrm{H}}\tilde{\boldsymbol{R}}^{-1}\tilde{\boldsymbol{P}}_i)^{-1}\tilde{\boldsymbol{P}}_i^{\mathrm{H}}\tilde{\boldsymbol{R}}^{-1}]\tilde{\boldsymbol{X}}_i$.

Substitute (16) and (17) into (15), and the persymmetric subspace polarimetric detector of range-spread targets based on GLRT (PerSPolGLRT) can be obtained as

$$\prod_{i=1}^{H}\frac{\sqrt{\boldsymbol{\Psi}_i^{(0)}(1,1)\boldsymbol{\Psi}_i^{(0)}(2,2)}+\mathrm{Re}(\boldsymbol{\Psi}_i^{(0)}(1,2))}{\sqrt{\boldsymbol{\Psi}_i^{(1)}(1,1)\boldsymbol{\Psi}_i^{(1)}(2,2)}+\mathrm{Re}(\boldsymbol{\Psi}_i^{(1)}(1,2))}\underset{\mathrm{H}_0}{\overset{\mathrm{H}_1}{\gtrless}}\eta_{\mathrm{PerSPolGLRT}}. \tag{18}$$

3.2 Polarimetric detector based on the Rao test

First, we give some notations as follows:

(i) the covariance matrix $\boldsymbol{R}$ is known;

(ii) $\tau_{\mathrm{HH}},\tau_{\mathrm{HV}}$, and $\boldsymbol{B}_1,\boldsymbol{B}_2,\cdots,\boldsymbol{B}_H$ are unknown parameters;

(iii) $\boldsymbol{\theta}_r=[\boldsymbol{\theta}_{r,1}^{\mathrm{T}},\boldsymbol{\theta}_{r,2}^{\mathrm{T}},\cdots,\boldsymbol{\theta}_{r,H}^{\mathrm{T}}]^{\mathrm{T}}$, where $\boldsymbol{\theta}_{r,i}=[b_{\mathrm{R},i,1},b_{\mathrm{R},i,2},\cdots,b_{\mathrm{R},i,2N_i},b_{\mathrm{I},i,1},b_{\mathrm{I},i,2},\cdots,b_{\mathrm{I},i,2N_i}]^{\mathrm{T}}$, $b_{\mathrm{R},i,n}$ and $b_{\mathrm{I},i,n}$ are the real and the imaginary parts of $b_{i,n}$ $(i=1,2,\cdots,H;n=1,2,\cdots,2N_i)$;

(iv) $\boldsymbol{\theta}_s=[\boldsymbol{\theta}_{s,1}^{\mathrm{T}},\boldsymbol{\theta}_{s,2}^{\mathrm{T}},\cdots,\boldsymbol{\theta}_{s,H}^{\mathrm{T}}]^{\mathrm{T}}$, where $\boldsymbol{\theta}_{s,i}=[\tau_{\mathrm{HH},i},\tau_{\mathrm{HV},i}]^{\mathrm{T}}$;

(v) $\boldsymbol{\theta}=[\boldsymbol{\theta}_r^{\mathrm{T}},\boldsymbol{\theta}_s^{\mathrm{T}}]^{\mathrm{T}}$ contains all unknown parameters.

Rao test for the problem of interest is given by

$$\left.\frac{\partial\ln f(\tilde{x}_{11},\tilde{x}_{21},\cdots,\tilde{x}_{H1}\mid\boldsymbol{\theta})}{\partial\boldsymbol{\theta}_r}\right|_{\boldsymbol{\theta}=\hat{\boldsymbol{\theta}}_0}^{\mathrm{T}}\left[\boldsymbol{J}^{-1}\left(\hat{\boldsymbol{\theta}}_0\right)\right]_{\theta_r,\theta_r}\cdot\left.\frac{\partial\ln f(\tilde{x}_{11},\tilde{x}_{21},\cdots,\tilde{x}_{H1}\mid\boldsymbol{\theta})}{\partial\boldsymbol{\theta}_r}\right|_{\boldsymbol{\theta}=\hat{\boldsymbol{\theta}}_0}\underset{\mathrm{H}_0}{\overset{\mathrm{H}_1}{\gtrless}}\eta \tag{19}$$

where $\hat{\boldsymbol{\theta}}_0$ is the maximum likelihood estimation of $\boldsymbol{\theta}$ under the H_0 hypothesis, $f(\tilde{x}_{11},\tilde{x}_{21},\cdots,\tilde{x}_{H1}\mid\boldsymbol{\theta})$ is the PDF of $\tilde{\boldsymbol{x}}_1,\tilde{\boldsymbol{x}}_2,\cdots,\tilde{\boldsymbol{x}}_H$ under the H_1 hypothesis, $\boldsymbol{J}$ is the Fisher information matrix, which can be partitioned as

$$\boldsymbol{J}(\theta)=\left[\begin{array}{cc}\boldsymbol{J}_{\theta_r,\theta_r}(\boldsymbol{\theta}) & \boldsymbol{J}_{\theta_r,\theta_s}(\boldsymbol{\theta})\\ \boldsymbol{J}_{\theta_s,\theta_r}(\boldsymbol{\theta}) & \boldsymbol{J}_{\theta_s,\theta_s}(\boldsymbol{\theta})\end{array}\right] \tag{20}$$

where $[\boldsymbol{J}^{-1}(\boldsymbol{\theta})]_{\theta_r,\theta_r}=(\boldsymbol{J}_{\theta_r,\theta_r}(\boldsymbol{\theta})-\boldsymbol{J}_{\theta_r,\theta_s}(\boldsymbol{\theta})\boldsymbol{J}_{\theta_s,\theta_s}^{-1}(\boldsymbol{\theta})\boldsymbol{J}_{\theta_s,\theta_r}(\boldsymbol{\theta}))^{-1}$.

After algebraic manipulations, the persymmetric subspace signal polarimetric detector of range-spread targets based on the Rao test (PerSPolRAO) can be obtained as

$$\sum_{i=1}^{H}\tilde{\boldsymbol{x}}_i^{\mathrm{H}}\boldsymbol{\Gamma}_{i,0}^{-1}\tilde{\boldsymbol{R}}^{-1}\tilde{\boldsymbol{P}}_i(\tilde{\boldsymbol{P}}_i^{\mathrm{H}}\tilde{\boldsymbol{R}}^{-1}\tilde{\boldsymbol{P}}_i)^{-1}\tilde{\boldsymbol{P}}_i^{\mathrm{H}}\tilde{\boldsymbol{R}}^{-1}\boldsymbol{\Gamma}_{i,0}^{-1}\tilde{\boldsymbol{x}}_i\underset{\mathrm{H}_0}{\overset{\mathrm{H}_1}{\gtrless}}\eta_{\mathrm{PerSPolRAO}} \tag{21}$$

where $\boldsymbol{\Gamma}_{i,0}$ is the maximum likelihood estimation of $\boldsymbol{\Gamma}_i$ under the H_0 hypothesis.

3.3 Polarimetric detector based on the Wald test

Similar to Rao test, we also suppose that $\tilde{\boldsymbol{R}}$ is known. The Wald test for the problem of interest is the following decision rule:

$$\hat{\boldsymbol{\theta}}_{r,1}^{\mathrm{T}}\left(\left[\boldsymbol{J}^{-1}\left(\hat{\boldsymbol{\theta}}_1\right)\right]_{\theta_r,\theta_r}\right)^{-1}\hat{\boldsymbol{\theta}}_{r,1}\underset{\mathrm{H}_0}{\overset{\mathrm{H}_1}{\gtrless}}\eta \tag{22}$$

where $\hat{\boldsymbol{\theta}}_1=[\hat{\boldsymbol{\theta}}_{r1}^{\mathrm{T}},\hat{\boldsymbol{\theta}}_{s1}^{\mathrm{T}}]^{\mathrm{T}}$ and $\hat{\boldsymbol{\theta}}_{r1}=[\hat{\boldsymbol{\theta}}_{r1,1}^{\mathrm{T}},\hat{\boldsymbol{\theta}}_{r1,2}^{\mathrm{T}},\cdots,\hat{\boldsymbol{\theta}}_{r1,H}^{\mathrm{T}}]^{\mathrm{T}}$ are the maximum likelihood estimates of $\boldsymbol{\theta}$ and $\boldsymbol{\theta}_r$ under H_1 hypothesis, respectively.

After algebraic manipulations, the persymmetric subspace signal polarimetric detector of range-spread targets based on the Wald test (PerSPolWALD) can be obtained as follows:

$$\sum_{i=1}^{H}\left(\tilde{\boldsymbol{x}}_i^{\mathrm{H}}\boldsymbol{\Gamma}_{i,1}^{-1}\tilde{\boldsymbol{R}}^{-1}\tilde{\boldsymbol{P}}_i(\tilde{\boldsymbol{P}}_i^{\mathrm{H}}\tilde{\boldsymbol{R}}^{-1}\tilde{\boldsymbol{P}}_i)^{-1}\times\tilde{\boldsymbol{P}}_i^{\mathrm{H}}\tilde{\boldsymbol{R}}^{-1}\boldsymbol{\Gamma}_{i,1}^{-1}\tilde{\boldsymbol{x}}_i\right)\underset{\mathrm{H}_0}{\overset{\mathrm{H}_1}{\gtrless}}\eta_{\mathrm{PerSPolWALD}} \tag{23}$$

where $\boldsymbol{\Gamma}_{i,1}$ is the maximum likelihood estimation of $\boldsymbol{\Gamma}_i$ under the H_1 hypothesis.

Three detectors are proposed to process echoes from HH and HV channels. The speckle components of the sea

clutter received by the co-polarized channel (HH or VV) and cross-polarized channel (HV or VH) are independent, so the persymmetric property of the speckle covariance matrix can be used in the design of the polarization detector. The proposed detector can also process the data from HH and HV channels.

3.4 Adaptive detectors design

In order to make the derived detectors fully adaptive, we replace the covariance matrix $\boldsymbol{R}$ in (18), (21), and (23) with an estimate of $\tilde{\boldsymbol{R}}$ based on the secondary data. The approximate maximum likelihood estimator (AMLE) [2] is an iterative estimation method, and can balance the estimation performance and the calculation amount. In addition, it can guarantee the CFAR property with respect to the texture component and the speckle covariance matrix. Thus, the AMLE is adopted to estimate the covariance matrix $\boldsymbol{R}$ given by

$$\hat{\boldsymbol{R}}_{\mathrm{Pol,AMLE}}(m+1)=\frac{L}{N}\sum_{k=H+1}^{H+L}\frac{\boldsymbol{x}_{\mathrm{Pol},k}\boldsymbol{x}_{\mathrm{Pol},k}^{\mathrm{H}}}{\boldsymbol{x}_{\mathrm{Pol},k}\hat{\boldsymbol{R}}_{\mathrm{pol,AMLE}}(m)^{-1}\boldsymbol{x}_{\mathrm{Pol},k}^{\mathrm{H}}},\ \mathrm{Pol}=\mathrm{HH,HV} \tag{24}$$

where $m\geqslant 1$ is the number of iterations, the starting point of iteration is usually set as the normalized sample covariance matrix estimate, i.e., $\hat{\boldsymbol{R}}_{\mathrm{Pol,AMLE}}(0)=\hat{\boldsymbol{R}}_{\mathrm{Pol,NSCME}}$. The estimate of the speckle covariance matrix of sea clutter is transformed as

$$\hat{\tilde{\boldsymbol{R}}}=\mathrm{Re}\left(\hat{\boldsymbol{R}}_{\mathrm{AMLE}}\{\tilde{\boldsymbol{x}}_1,\tilde{\boldsymbol{x}}_2,\cdots,\tilde{\boldsymbol{x}}_L\}\right)=\mathrm{Re}\left(\boldsymbol{W}_{\mathrm{Pol}}\hat{\boldsymbol{R}}_{\mathrm{AMLE}}\{\boldsymbol{x}_1,\boldsymbol{x}_2,\cdots,\boldsymbol{x}_L\}\boldsymbol{W}_{\mathrm{Pol}}^{\mathrm{H}}\right). \tag{25}$$

The fully adaptive detectors can be obtained by substituting the estimated value $\hat{\tilde{\boldsymbol{R}}}$ in (25) into (18), (21), and (23).

In the design of the above three detectors, the clutter texture is estimated by the radar echo data. Therefore, the test statistics are not affected by the fluctuation of the power level and are independent of the clutter texture distribution. Moreover, the explicit form of the probability of false alarm (PFA) cannot be given, the CFAR property of the three detectors with respect to the speckle covariance matrix is analyzed through the following Monte Carlo experiments.

The experimental parameters are set as: N=8, H=4, L=64, $P_{\mathrm{fa}}=10^{-4}$, and the speckle covariance matrix of each polarimetric channel is an exponential decay covariance matrix $[\boldsymbol{R}_{\mathrm{HH}}]_{i,j}=[\boldsymbol{R}_{\mathrm{HV}}]_{i,j}=\rho^{|i-j|}(1\leqslant i\leqslant j\leqslant N)$. In Fig.1(a), the PFA curves of three detectors are plotted with respect to the speckle covariance matrix. The detection threshold used in this experiment is obtained when $\rho=0$. From Fig.1(a), it can be seen that the PFA remains constant for different ρ. Fig. 1 (b) shows the PFA curves of the three detectors against AMLE. It can be found that the detectors are CFAR with respect to ρ.

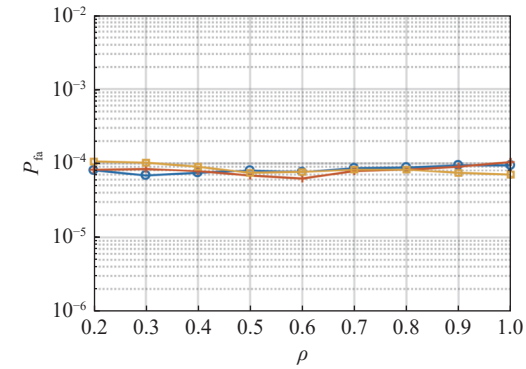

(a) Real $\boldsymbol{R}$

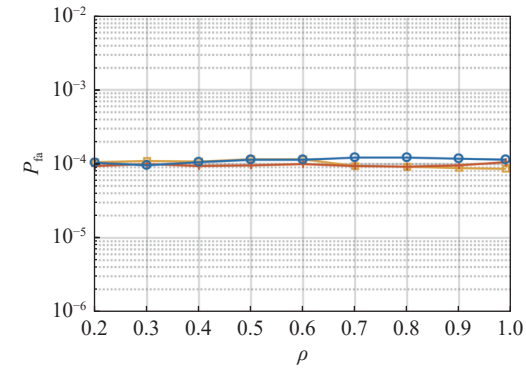

(b) AMLE

: PerSPolGLRT; : PerSPolRAO; : PerSPolWALD.

Fig. 1 PFA versus ρ

4. Performance assessment

In this section, we evaluate the performance of three detectors through the simulated and real radar data. The sea clutter is modeled by a K distribution, and thus clutter textures τ_{HH} and τ_{HV} obey the two parameter Gamma distribution, i.e., $\tau_{\mathrm{HH}}\sim\mathrm{Gamma}(\lambda_{\mathrm{HH}},\mu_{\mathrm{HH}})$, $\tau_{\mathrm{HV}}\sim\mathrm{Gamma}(\lambda_{\mathrm{HV}},\mu_{\mathrm{HV}})$. The PDF of Gamma distribution is given by

$$p(\tau)=\frac{\lambda^{\lambda}}{\Gamma(\lambda)\mu^{\lambda}}\tau^{\lambda-1}\exp\left(-\frac{\lambda}{\mu}\tau\right) \tag{26}$$

where μ is the scale parameter, reflecting the average clutter power, and λ is the shape parameter describing the non-Gaussian characteristics of sea clutter. We set the clutter parameters of the two polarimetric channels as $\lambda_{\mathrm{HH}}=\lambda_{\mathrm{HV}}$, $\mu_{\mathrm{HH}}=\varepsilon\mu_{\mathrm{HV}}$, and $P_{\mathrm{fa}}=10^{-4}$, where ε is the scale factor. The detection threshold is obtained by 10^6 independent Monte Carlo experiments. The

probability of detection (Pd) corresponding to different average signal-to-clutter ratios (A-SCR) is calculated by 5 000 independent experiments. The A-SCR in the experiment is defined as follows:

$$\text{A-SCR} = \frac{\sum_{i=1}^{H} (\boldsymbol{E}_i \boldsymbol{a}_i)^{\mathrm{H}} (\boldsymbol{E}_i \boldsymbol{a}_i)}{NH(\mu_{\mathrm{HH}} + \mu_{\mathrm{HV}})}. \tag{27}$$

In the experiment, the signal amplitude of different scatters in each polarimetric channel is assumed to be the same between pulses. Table 1 shows the used target subspace models, where M1 represents the range spread target of rank one, and M2 represents the range spread target of multiple ranks. The values in the table represent the normalized Doppler frequencies of different scattering centers .

Table 1 Distribution of scatters in Doppler dimension in each range cell of the range-spread target

Target model	Target cell			
	1	2	3	4
M1	0.1	0.1	0.1	0.1
M2	0.1,0.2	0.2	0.2,0.4	0.1,0.2,0.3,0.4

The traditional detectors for comparison in the experiment include the range-spread target polarimetric detector PolGLRT [30] using the rank one target model and the subspace range spread target detector ARDTD [16]. The test statistic form of PolGLRT is similar to PerSPolGLRT. The ARDTD is given by

$$\sum_{i=1}^{H} \frac{\boldsymbol{x}_i^{\mathrm{H}} \hat{\boldsymbol{D}}_i \boldsymbol{x}_i}{\boldsymbol{x}_i^{\mathrm{H}} \hat{\boldsymbol{R}}^{-1} \boldsymbol{x}_i} \underset{\mathrm{H}_0}{\overset{\mathrm{H}_1}{\gtrless}} \eta_{\mathrm{ARDTD}} \tag{28}$$

where $\hat{\boldsymbol{D}}_i = \hat{\boldsymbol{R}}^{-1}\boldsymbol{U}_i(\boldsymbol{U}_i^{\mathrm{H}}\hat{\boldsymbol{R}}^{-1}\boldsymbol{U}_i)^{-1}\boldsymbol{U}_i^{\mathrm{H}}\hat{\boldsymbol{R}}^{-1}$, $\boldsymbol{x}_i$ represents the echo of a single polarimetric channel, $\boldsymbol{R}$ represents the speckle covariance matrix of a single polarimetric channel. In the experiments, PolGLRT and ARDTD will process the radar echoes from the HV channel.

4.1 Performance assessment of simulation data

In Fig. 2, the detection performance of the proposed three detectors and PolGLRT with the M1 target model is compared under different numbers of the secondary cell. The experimental parameters are set as $\lambda_{\mathrm{HH}} = \lambda_{\mathrm{HV}} = 3$, $\mu_{\mathrm{HH}} = 1$, $\rho = 0.9$, $\varepsilon = 0.5$. $\varepsilon = 0.5$ indicates that the A-SCR in the HV channel is about 3 dB higher than that in the HH channel. It can be found from Fig. 2 (a) that when L=8, the Pd of PolGLRT detector is only 0.04 when A-SCR is 10 dB. In contrast, the proposed PerSPolGLRT, PerSPolRAO, and PerSPolWALD have better performance. When the SCR reaches 8 dB, the Pd is almost 1. Fig. 2 (b) shows that when L=16, the performance of the PolGLRT detector has been greatly improved, but it is still not beyond the three proposed detectors. When the Pd is 0.9, the performance gain of PerSPolGLRT, and PerSPolRAO is about 3 dB in Fig. 2 (b). Fig. 2 (c) and Fig. 2 (d) show that the curve of the PolGLRT detector approaches three polarimetric detectors when L=32 and L=64, respectively. For the different numbers of secondary data, the Pds of PerSPolGLRT and PerSPolRAO are almost the same and higher than that of PerSPolWALD.

Fig. 3 shows the detection performance of all detectors using the M2 target model. It indicates that the performance of PerSPolGLRT is the best, and the ARDTD performs worst. When the number of secondary cells is 16 and the Pd is 0.9, compared with the ARDTD, the performance gain of PerSPolGLRT is 8 dB higher than that of ARDTD, and the performance gain of PerSPolRAO and PerSPolWALD are 5 dB and 6 dB, respectively. Moreover, as the number of secondary cells increases, the performance of ARDTD gradually approaches PerSPolWALD. The proposed three detectors are less dependent on secondary data, and thus are more suitable for target detection in non-homogeneous sea clutter.

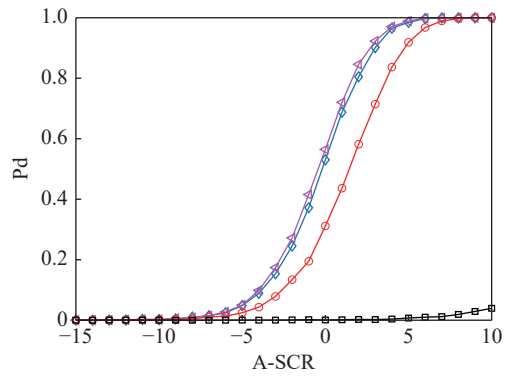

(a) L=8

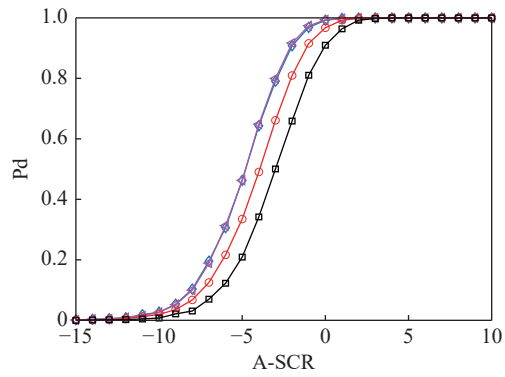

(b) L=16

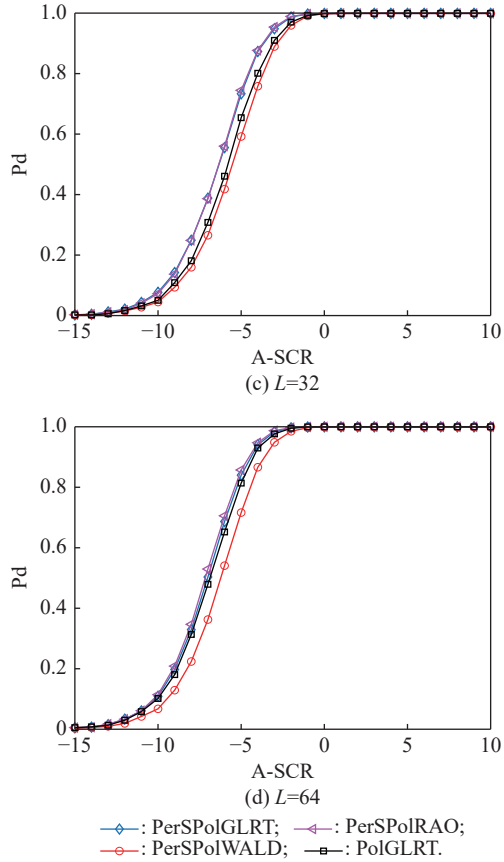

Fig. 2 Pd versus A-SCR plots of different number of secondary cells under target M1 model

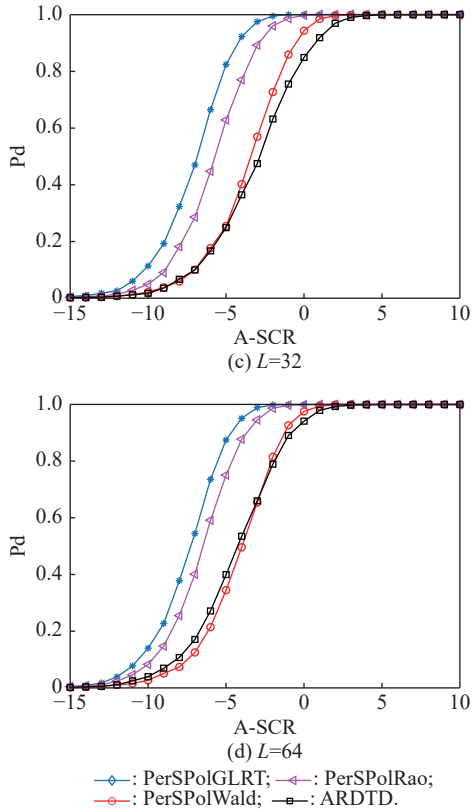

Fig. 3 Pd versus A-SCR plots of different number of secondary cells under target M2 model

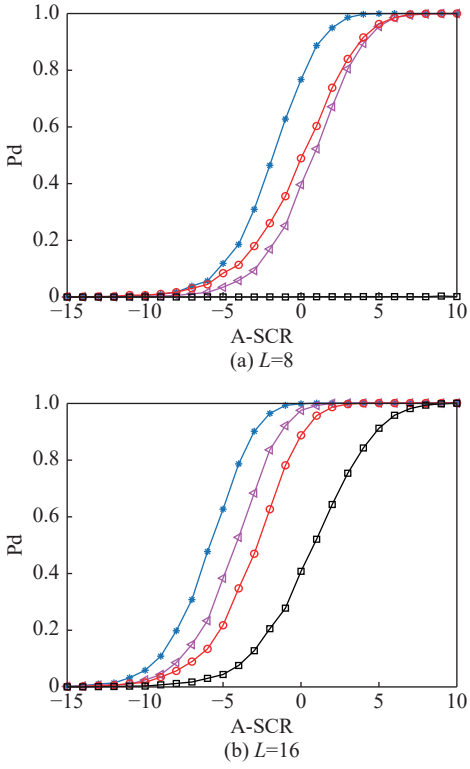

Fig. 4 analyzes the influence of shape parameters on the Pd of the three detectors using the M1 target model. Fig. 4 shows that the detection performance of three detectors is the best in the case of $\lambda = 1$, and the detection performance decreases with the increase of shape parameters. This result indicates that three polarimetric adaptive detectors have better detection performance in the non-Gaussian sea clutter background.

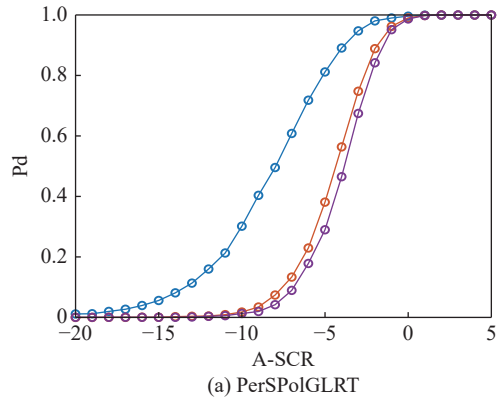

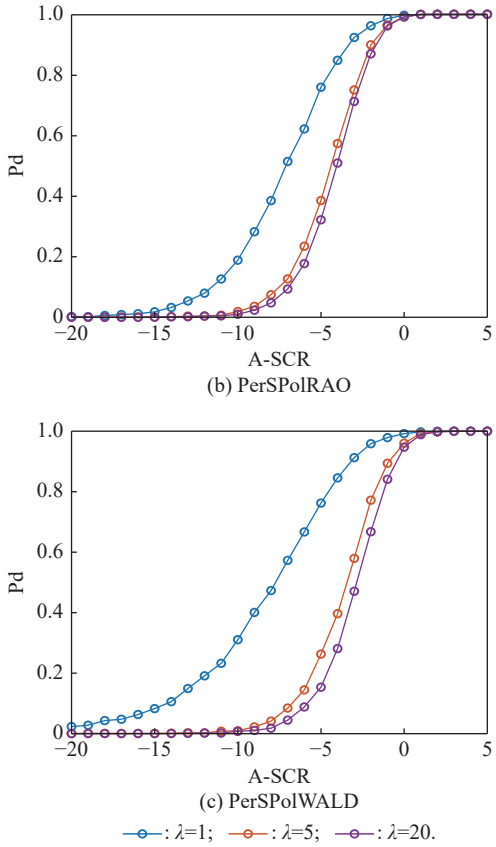

Fig. 4 Pd versus A-SCR plots of different shape parameter

The difference of clutter power caused by different polarimetric characteristics is also an important factor in the Pd. Fig. 5 displays the influence of ε on the Pd of the three detectors under the M1 target model. Fig. 5 (a) shows the situation at $\varepsilon = 0.01$, which means that the SCR in the HV channel is 20 dB higher than that in the HH channel, and the echoes from the HV channel obviously contribute more to the target detection. In Fig. 5 (a), it can be found that the Pd of the PolGLRT detector which processes the echoes from the HH and HV channels exceeds that of PerSPolWALD, but it is still slightly lower than that of PerSPolGLRT and PerSPolRAO, which have the strongest detection capability. With the increase of ε, the power difference between the two channels becomes smaller, and the advantages of the proposed polarimetric detectors are still obvious. Furthermore, we can see from Fig. 5(d) that the performance gain of PerSPolGLRT and PerSPolRAO is about 2 dB compared to PolGLRT when Pd is 0.9.

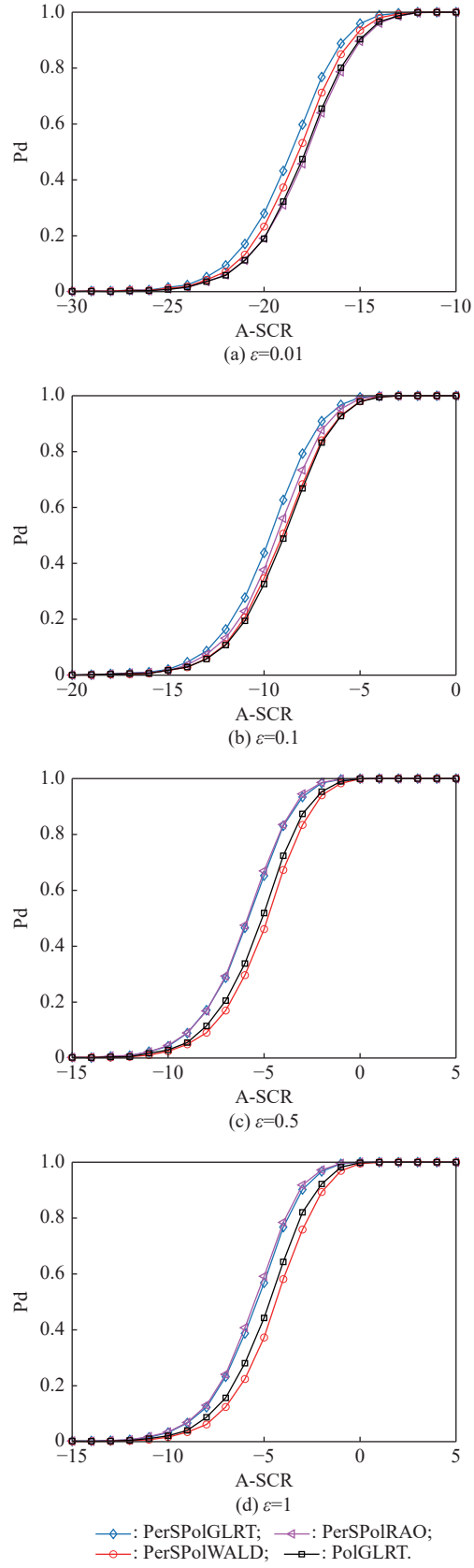

Fig. 5 Pd versus A-SCR plots of different ε under target M1 model

Fig. 6 shows the Pd curves of all detectors using the M2 target model. It can be found that the performance improvement of the proposed detector mainly comes from the use of polarization information. Note that from the experiment of M1, when the secondary data is sufficient, the improvement brought by the persymmetric structure is small. It should be noted here that $\varepsilon = 0.01$ is a limiting case assumed for performance analysis.

In addition to the above factors, the Pd is also affected by the center Doppler frequency of the target. Due to this reason, a more general "class M2" target model is defined [17]. The M2 target model in Table 1 belongs to a special case of this model. The distribution of the normalized Doppler frequency of each scatterer of "class M2" targets in the four CUTs is $\{f_{dc}-\Delta f_d, f_{dc}\}$, f_{dc}, $\{f_{dc}, f_{dc}+2\Delta f_d\}$, $\{f_{dc}-\Delta f_d, f_{dc}, f_{dc}+\Delta f_d, f_{dc}+2\Delta f_d\}$, where f_{dc} represents the center Doppler frequency shared by all range cells, Δf_d represents the spread of the target in the Doppler dimension.

Because the normalized Doppler frequency is varied within $[-0.5,0.5]$, we set $f_{dc} \in [-0.4,0.3]$ in Fig. 7. The A-SCR of the target to be detected is set as: A-SCR= −7 dB. The true value of the covariance matrix is used in the detection, and other parameter settings are the same as those in Fig. 3.

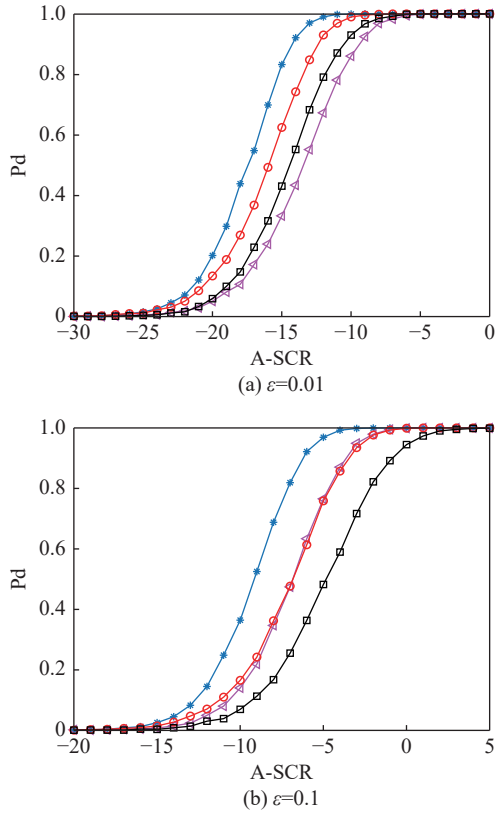

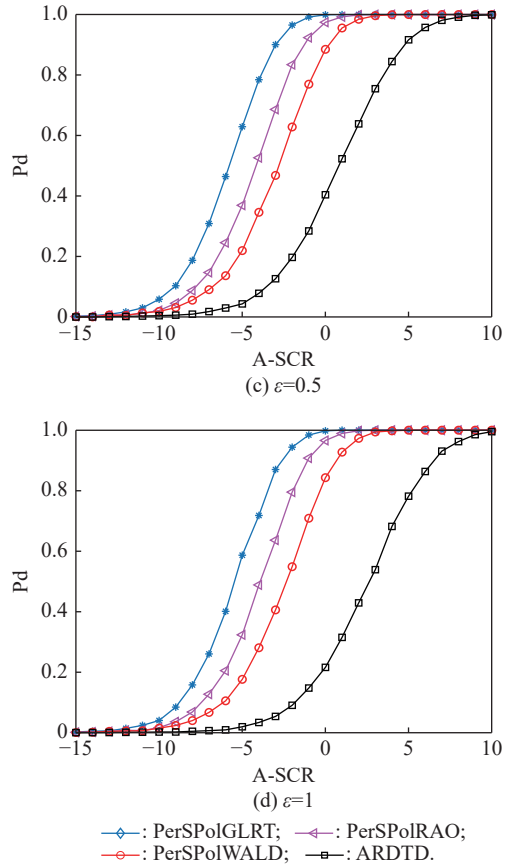

Fig. 6 Pd versus A-SCR plots of different ε under target M2 model

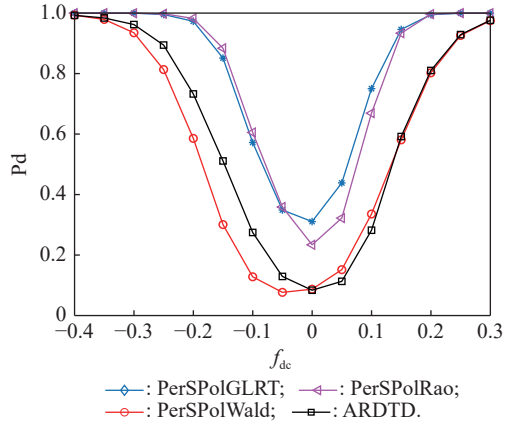

Fig. 7 Pd versus target center Doppler frequency plots

Fig. 7 shows the influence of the target center Doppler frequency on the Pd. It can be seen that the performance of four detectors at zero frequency has been seriously degraded. The reason is that the clutter energy is concentrated near the zero frequency. Therefore, the detection of low-speed targets usually requires a higher SCR. With the change of the central Doppler frequency, the Pds of PerSPolGLRT and PerSPolRAO are higher than the

ARDTD. However, in the central Doppler frequency interval of [−0.4,0], the Pd of PerSPolWALD is lower than ARDTD. In other intervals, the performance of the two is similar. Because the true value of the speckle covariance matrix is used in the experiment, so the upper bound of the performance of PerSPolWALD is not higher than ARDTD. With sufficient secondary data, the detection probabilities of the two are close, which is consistent with the performance curve in Fig. 3(d).

4.2 Performance assessment on measured data

In order to further verify the performance of three detectors, we adopt the measured radar data collected by the IPIX radar of McMaster University in 1998 [31]. The data file 19980212_195704_ANTSTEP is selected, where the range resolution is 15 m, the pulse repetition frequency is 1 000 Hz, and echoes of four polarimetric channels are included. We have processed the data of HH and HV channels to verify the proposed detectors. Fig. 8 shows the fitting results of the measured data by using different amplitude distributions. It can be seen that the K distribution has a good fitting for the data.

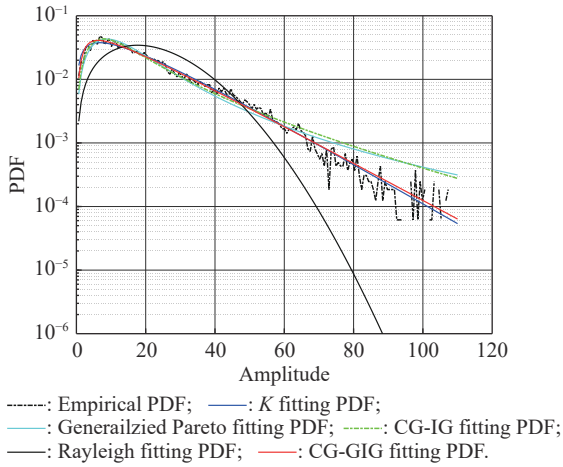

Fig. 8 Amplitude probability density function fitting of measured data 119980212_195704_ANTSTEP

In the experiments, we first remove the original target echo data and then select four range cells to add the simulated target signal. Fig. 9 shows the performance curves of three detectors, the PolGLRT detector and the ARDTD detectors using the M1 and M2 target models. It can be seen from Fig. 9(a) that the performance of PerSPolRAO and PerSPolGLRT is close and best, and is followed by that of PerSPolWALD. The performance of PerSPolGLRT and PerSPolRAO is better than that of PolGLRT. For multi-rank range-spread targets, the advantages of the three proposed detectors are more obvious. We can also find from Fig. 9(b) that the performance of PerSPolGLRT is the best, and is followed by PerSPolWALD, then PerSPolRAO. In addition, the Pd of the three detectors is much higher than that of ARDTD. When the Pd is 0.9, the performance gain of PerSPolGLRT is about 10 dB compared with ARDTD.

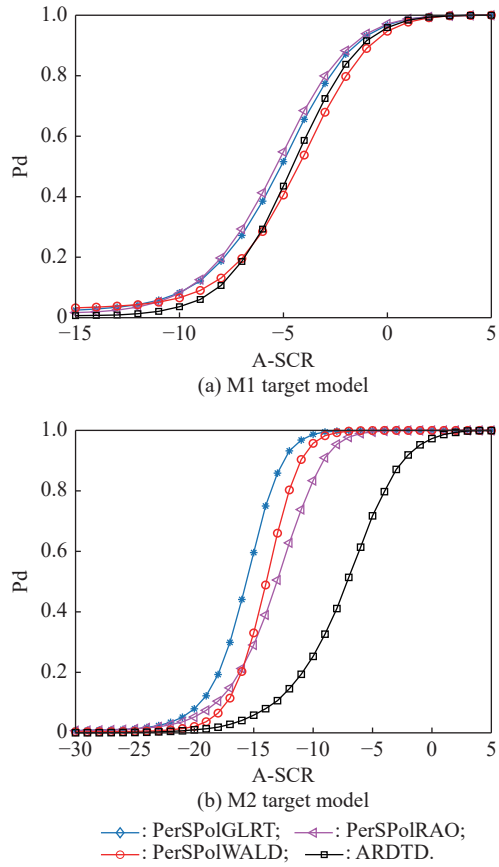

Fig. 9 Pd versus A-SCR plots of different target model under measured data

5. Conclusions

In this paper, the problem of the detection of range and Doppler dual-spread targets in the non-homogeneous and non-Gaussian sea clutter is considered. Three adaptive polarimetric adaptive detectors are proposed by using the GLRT, the Wald test, and the Rao test, respectively. The proposed detectors have the CFAR property with respect to texture distribution, and the speckle covariance matrix. Experiment results based on simulated and measured data show that the performance of the proposed PerSPolGLRT, PerSPolRAO, and PerSPolWALD is better than that of the traditional detectors. All the proposed detectors rely less on secondary data and are suitable for target detection in non-homogeneous and non-Gaussian environments.

References

[1] CONTE E, BISCEGLIE M D, GALDI C, et al. A procedure for measuring the coherence length of the sea texture. IEEE Trans. on Instrumentation and Measurement, 1997, 46(4): 836–841.

[2] GINI F, GRECO M. Covariance matrix estimation for CFAR detection in correlated heavy tailed clutter. Signal Processing, 2002, 82(12): 1847–1859.

[3] JAVIER C, JAVIER G, ÁLVARO B, et al. Statistical analysis of a high-resolution sea-clutter database. IEEE Trans. on Geoscience and Remote Sensing, 2010, 48(4): 2024–2037.

[4] WARD K D. Compound representation of high resolution sea clutter. Electronics Letters, 1981, 17(16): 561–563.

[5] CONTE E, LONGO M, LOPS M. Modelling and simulation of non-Rayleigh radar clutter. IEE Proceedings F (Radar and Signal Processing), 1991, 138(2): 121–130.

[6] JEN K J. Amplitude distribution of composite terrain radar clutter and the K-distribution. IEEE Trans. on Antennas & Propagation, 1984, 32(10): 1049–1062.

[7] GRECO M, STINCO P, GINI F. Identification and analysis of sea radar clutter spikes. IET Radar, Sonar & Navigation, 2010, 4(2): 239–250.

[8] FARSHCHIAN M, POSNER F L. The Pareto distribution for low grazing angle and high resolution X-band sea clutter. Proc. of the IEEE Radar Conference, 2010: 789−793.

[9] OLLILA E, TYLER D E, KOIVUNEN V, et al. Compound-Gaussian clutter modeling with an inverse Gaussian texture distribution. IEEE Signal Processing Letters, 2012, 19(12): 876–879.

[10] XUE J, XU S W, LIU J, et al. Model for non-Gaussian sea clutter amplitudes using generalized inverse Gaussian texture. IEEE Geoscience and Remote Sensing Letters, 2018, 16(6): 892–896.

[11] SHI S N, SHUI P L. Sea-surface floating small target detection by one-class classifier in time-frequency feature space. IEEE Trans. on Geoscience and Remote Sensing, 2018, 56(11): 6395–6411.

[12] PARK H R, LI J, WANG H. Polarimetric-space-time domain generalized likelihood ratio detection of radar targets. Signal Processing, 1995, 41(2): 153–164.

[13] ANTONIO D M, GIUSEPPE R. A polarimetric adaptive matched filter. Signal Processing, 2001, 81(12): 2583–2589.

[14] LOMBARDO P, PASTINA D, BUCCIARELLI T. Adaptive polarimetric target detection with coherent radar. II. Detection against non-Gaussian background. IEEE Trans. on Aerospace and Electronic Systems, 2001, 37(4): 1207–1220.

[15] DE M A, ALFANO G, CONTE E. Polarimetric diversity detection in compound-Gaussian clutter. IEEE Trans. on Aerospace and Electronic Systems, 2004, 40(1): 114–131.

[16] GUAN J, ZHANG Y F, HUANG Y. Adaptive subspace detection of range-distributed target in compound-Gaussian clutter. Digital Signal Processing, 2009, 19(1): 66–78.

[17] XU S W, SHI X Y, XUE J, et al. Adaptive subspace detection of range-spread target in compound Gaussian clutter with inverse Gaussian texture. Digital Signal Processing, 2018, 81: 79–89.

[18] SHUAI X F, KONG L J, YANG J Y. Performance analysis of GLRT-based adaptive detector for distributed targets in compound-Gaussian clutter. Signal Processing, 2010, 90(1): 16–23.

[19] ALFANO G, DE M A, CONTE E. Polarimetric diversity detection of distributed targets in compound-Gaussian clutter. IEEE Trans. on Aerospace and Electronic Systems, 2004, 40(2): 755–765.

[20] REED I S, MALLETT J D, BRENNAN L E. Rapid convergence rate in adaptive arrays. IEEE Trans. on Aerospace & Electronic Systems, 1974, AES-10(6): 853–863.

[21] PASTINA D, LOMBARDO P, BUCCIARELLI T. Adaptive polarimetric target detection with coherent radar. I. Detection against Gaussian background. IEEE Trans. on Aerospace and Electronic Systems, 2001, 37(4): 1194–1206.

[22] NITZBERG R. Application of maximum likelihood estimation of persymmetric covariance matrices to adaptive processing. IEEE Trans. on Aerospace and Electronic Systems, 1980, 16(1): 124–127.

[23] ZHANG Y X, SHU Q Q, JIANG T. A GLRT-based polarimetric detector for sea-surface weak target detection. IEEE Geoscience and Remote Sensing Letters, 2020, 19: 1500705.

[24] WANG Z H, HE Z S, HE Q, et al. Persymmetric adaptive CFAR detector in compound Gaussian sea clutter with inverse Gaussian texture. Proc. of the IEEE International Geoscience and Remote Sensing Symposium, 2021: 5000−5003.

[25] NOVAK L M, BURL M C. Optimal speckle reduction in POL-SAR imagery and its effect on target detection. Proc. of the SPIE Technical Symposium on Aerospace Sensing, 1989: 84–115.

[26] WAX M, ZISKIND I. Detection of the number of coherent signals by the MDL principle. IEEE Trans. on Acoustics, Speech, and Signal Processing, 1989, 37(8): 1190–1196.

[27] WAX M. Detection and localization of multiple sources in noise with unknown covariance. IEEE Trans. on Signal Processing, 1992, 40(1): 245–249.

[28] MA C, NG B P. A CFAR based model order selection criterion for complex sinusoids. Signal Processing, 2006, 86(9): 2296–2303.

[29] NICOLAS B, KHENCHARF A, GARELLO R. GLRT subspace detection for range and Doppler distributed targets. IEEE Trans. on Aerospace and Electronic Systems, 2008, 44(2): 678–696.

[30] CUI G L, KONG L J, YANG X B, et al. Distributed target detection with polarimetric MIMO radar in compound-Gaussian clutter. Digital Signal Processing, 2012, 22(3): 430–438.

[31] HAYKIN S. The McMaster IPIX radar sea clutter database. http://soma.crl.mcmaster.ca/ipix/.

Biographies

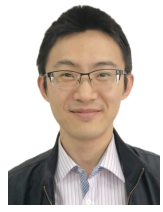

XU Shuwen was born in 1985. He received his B.E. and Ph.D. degrees in electronic engineering from Xidian University, Xi ’an, China, in 2006 and 2011, respectively. He is a professor with the National Key Laboratory of Radar Signal Processing, Xidian University. His research interests are in the fields of radar target detection, time-frequency analysis, and synthetic aperture radar image processing.

E-mail: swxu@mail.xidian.edu.cn

HAO Yifan was born in 1997. He received his M.S. degree in information and communication engineering from Xidian University. He is an assistant engineer in Xi ’an Electronic Engineering Research Institute. His research interests include polarimetric adaptive detection and sea clutter characteristic analysis.
E-mail: yf_hao@stu.xidian.edu.cn

WANG Zhuo was born in 1980. He received his M.S. degree in information and communication engineering from Xidian University. He is a researcher with Beijing Institute of Radio Measurement, Beijing, China. His research interests include radar system design and signal processing.
E-mail: kingwz301@sina.com

XUE Jian was born in 1993. He received his B.E. and Ph.D. degrees in electronic engineering from Xidian University, Xi ’an, China, in 2015 and 2020, respectively. He is an associate professor with the School of Communications and Information Engineering, Xi ’an University of Posts and Telecommunications. His research interests include radar clutter suppression, radar target detection, machine learning, and intelligent radar signal processing.
E-mail: jxue@xupt.edu.cn